Bedrock incision modeling and threshold slope development in a variable tectonic regime, Namche Barwa Region, SE Tibet

Eric F. Buer

A thesis submitted in partial fulfillment of the
requirements for the degree of

Master of Science

University of Washington

2007

Program Authorized to Offer Degree:
Department of Earth and Space Sciences

University of Washington
Graduate School

This is to certify that I have examined this copy of a master's thesis by

Eric F. Buer

and have found that it is complete and satisfactory in all respects,
and that any and all revisions required by the final
examining committee have been made.

Committee Members:

_____

David R. Montgomery

_____

Charles A. Nittrouer

_____

Gerard H. Roe

Date:_____

Signature_____

Date_____

University of Washington

Abstract

Bedrock incision modeling and threshold slope development in a variable tectonic regime, Namche Barwa Region, SE Tibet

Eric F. Buer

Chair of the Supervisory Committee:
David R. Montgomery, Professor
Department of Earth and Space Sciences

Digital elevation model (DEM) analysis of the Namche Barwa region of the Himalaya, SE Tibet, was paired with new mineral cooling ages to examine assumptions common to many current bedrock incision models and investigate the development of landscapes in a variable tectonic environment. Apatite fission track, $^{40}Ar/^{39}Ar$ Biotite and (U-Th)/He Zircon ages were used to determine general rates of rock exhumation in the region. Bedrock channel profiles derived from the DEM were then examined in these tectonic regimes. A strong correlation between channel steepness (k_s) and concavity (θ) values was found to persist across a wide range of exhumation rates and hypothesized to result from a coupling between the influence of debris flow and fluvial processes on bedrock river incision. Channel steepness k_s and mean hillslope gradients of fluvial watersheds were correlated up to a slope of approximately 30° but showed no relationship in steeper catchments.

TABLE OF CONTENTS

LIST OF FIGURES

LIST OF TABLES

ACKNOWLEDGEMENTS

There are many people to whom I owe a deep debt of gratitude. I wish to thank my committee members Dave Montgomery, Gerard Roe and Chuck Nittrouer for providing me with both encouragement and support that has made a world of difference in every step of my graduate work. I would also like to thank Harvey Greenberg for his exceptional technical support, and without whom I am convinced I would have been mired in low productivity frustration when performing the DEM analysis portion of this paper. Throughout the time I have worked on this manuscript, I have been blessed with the ongoing support of my family and friends. I wish to extend my deepest and most heartfelt thanks to all of them and particularly to my parents Stein and Noelle, and my girlfriend Laura.

Introduction

In this study, we use tributaries to the Tsangpo River in the eastern Himalaya to obtain stream profiles for watersheds with a wide range of rock exhumation rates. We use these watersheds to examine assumptions common to many models of channel incision and investigate threshold hillslope development. Two important properties of channels are their indices of steepness (k_s) and concavity (θ) (Whipple and Tucker, 1999). Researchers using traditional models of fluvial incision in the interpretation of many landscapes (e.g., Howard et al., 1994; Sklar and Dietrich, 1998; Kirby et al., 2003; and others) have noted that k_s and θ show strong covariance among profiles as a function of the mathematical relationship describing individual channel profiles. Subsequent research (e.g., Snyder et al., 2000; Kirby et al., 2003) has generally accepted the covariance between k_s and θ, but noted that the range of θ values was small. Thus, the practice of using a fixed θ value to normalize k_s has become a commonly accepted method to facilitate interbasin comparisons. Our analysis of Advanced Spacebourne Thermal Emission and Reflection Radiometry (ASTER) digital elevation models (DEM) presents a new set of observed θ and k_s values that demonstrate the predicted covariance, and imply the influence of variable erosive processes on the channels in this region. New mineral cooling age data in the region (Zeitler, unpublished data) have been used to determine general exhumation rates over the study area, allowing us to address further the relationship between tectonics, k_s, and erosive process for bedrock channels.

We also use our watershed data to evaluate the relationship between channel incision, and surrounding topographic development as seen in hillslope gradient.

Previous studies (Burbank et al., 1996; Montgomery, 2001; Montgomery and Brandon, 2002; Binnie et al., 2007, Korup et al., 2007) have addressed the development of threshold landscapes as a balance between erosion of the landscape and tectonic uplift, which allows new rock to replace material removed by erosion at the earth's surface. Here, we specifically investigate the transition between dominant processes that control development of surface relief as the local tectonic regime changes from low exhumation rates on the Tibetan Plateau to high exhumation rates in the region surrounding the Tsangpo River gorge (Zeitler et al., 2001).

Study Area

The Himalayan Mountains were formed as part of an intercontinental collision between India and mainland Asia which began approximately 55 Ma (Harrison et al., 1997). The mountain belt comprises roughly one third of the total collision zone (Zeitler et al., 2001) and has a mean elevation of 5 kilometers, comparable to that of the Tibetan Plateau. Previous studies focusing on erosion in the Himalaya have taken advantage of both the eastern and western syntaxis, where river incision rates range from <2 mm yr^{-1} to as much as 12 mm yr^{-1} depending on location (Burbank et al., 1996; Zeitler et al., 2001). In our study area, localized erosion rates of up to 5 mm yr^{-1} have been observed as part of a concentrated zone of higher-temperature material experiencing both rapid uplift and rapid erosion that forms a bull's eye pattern centered over Namche Barwa (Zeitler et al., 2001). This "tectonic aneurysm" provides us an ideal opportunity to examine bedrock channel response to a range of uplift rates (which can be determined through mineral cooling ages), while limiting variation in aspects such as climate and changes in lithology, which are commonly combined in a single mathematical variable for modeling purposes.

Previous investigations into the rate of bedrock incision at the western syntaxis of the Himalaya postulated that bedrock hillslopes developed uniformly to a critical gradient of approximately 30 degrees (Burbank et al., 1996). Beyond this slope, further increases in exhumation rate are thought to increase landslide frequency which moderates relief development resulting from fluvial incision. Our study in the eastern Himalaya (Figure 1) presents an ideal environment in which to examine development of hillslope gradients in a wide range of long-term exhumation rates to further test the relationship between the

two.

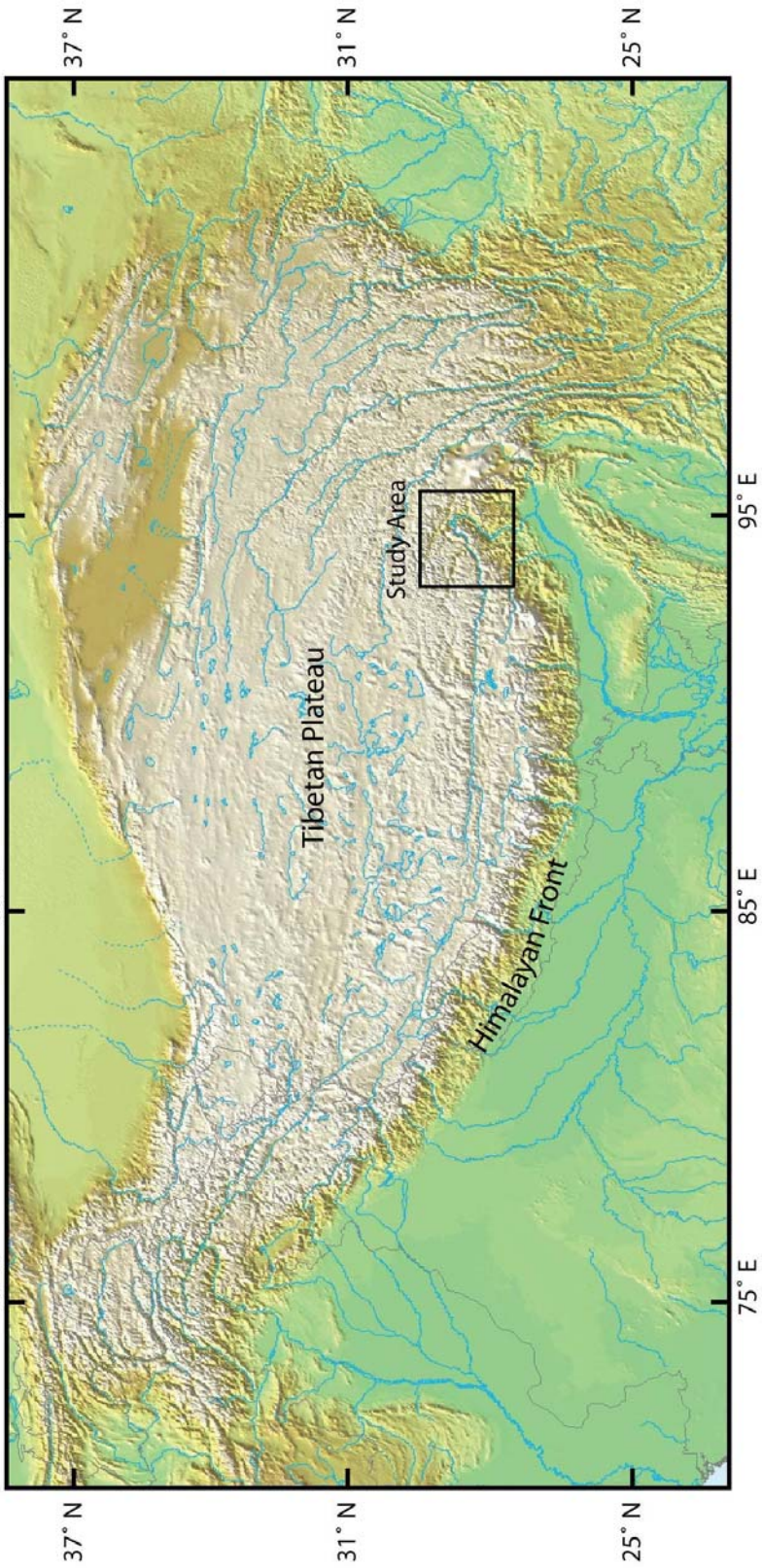

Figure 1. Study area location in the eastern Himalaya.

Methods

Calculation of Exhumation Rates

Calculation of local erosion rates depends on the thermal state of the crust. A general approximation of the thermal profile of the crust can be calculated using the formula for depth dependent temperature (Stuwe, 2002)

$$T(Z) = T_f\,(1 - e^{(-UZ/K)})/(1-e^{(UZ_0/K)}) \quad (1)$$

where T_f is a fixed temperature at some depth in the crust, U is the erosion rate in m yr^{-1} (later converted to mm yr^{-1} for our purposes), Z is the depth of interest in m, Z_0 is the depth of the crustal boundary and K is thermal diffusivity. Closure temperatures for mineral cooling ages have been previously established as follows: zircon (U-Th)/He closure temperatures are 185-210 °C (Reiners et al., 2002); $^{40}Ar/^{39}Ar$ biotite ages closure temperatures are 300-335 °C (Grove and Harrison, 1996); and apatite fission track closure temperature is 120 °C (Warnock et al., 1997). Depth of closure can be calculated using established closure temperatures, the measured mineral cooling age, and an initial presumed rate of erosion. This depth is then refined through an iterative process to match the known closure depth of each mineral and used to determine a final erosion rate. While the accuracy of this method is limited by several computational variables (including the number of iterations used to find the solution and the spatial resolution of the thermal profile), the method is sufficient for our purposes of distinguishing between watersheds with rapid and slow exhumation rates, and proved consistent between dating methods.

Isochron maps for each dating method were converted to generalized maps of exhumation rates using the method described above (Table 1). Exhumation rates based

on calculations using each method were then combined to form an overall exhumation rate map for the study area (Figure 2), which accounted for density of age data points, number of similar ages, etcetera. These exhumation rates are comparable to previous studies in the region (Zeitler, 2001) and are sufficient to discriminate between exhumation regimes (Table 2).

Each dating method closes at a unique depth, comparison of the closure ages for three different methods provides a set of "snapshots" into the rate of rock exhumation. Finding comparable rates of exhumation between closure depths indicates the rate of exhumation has remained constant as it passed through several depths, and provides strong evidence that the region has reached both erosional and thermal steady state. We use this assumption when addressing bedrock channel profiles and presume that because the rate of erosion has been held steady over a long period, bedrock channel incision has adjusted, and allowed topographic equilibrium to be reached.

DEM Analysis

Drainage area and slope data were assembled from watersheds in the study area using ASTER digital elevation models (DEM) with a spatial (grid cell) resolution of 15 m (Figure 3). Previous work found that longitudinal profiles developed from DEMs with a 10-m grid resolution were comparable to those calculated using surveyed longitudinal profiles or digitized topographic maps (e.g., Snyder et al. 2000). Hence, the 15-m DEM resolution was deemed adequate to apply similar analytical methods for this study. Initial locations were chosen to be roughly 10 km or less from any of the 52 mineral cooling age

sampling locations which were used to determine exhumation rates. Some mineral cooling samples are therefore associated with more than a single watershed.

Watershed morphology was inspected visually prior to numerical analysis to screen out those with obvious non-fluvial features such as glacial moraines, hanging valleys, or river profile setting landslides. Selected watersheds were then analyzed to calculate mean hillslope gradient and basin area, as well as the slope and drainage area for each pixel. The data cloud of slope-drainage data thus obtained was then reduced using log-bin averaging to produce a single curve of watershed drainage area versus slope, following methods widely employed in previous studies (e.g., Tarboton et al., 1989; Tarboton et al., 1991; Snyder et al., 2000, Montgomery, 2001). Power-law regression analysis of the resulting data defining an area-slope curve was then used to determine the values of k_s and θ. Each channel profile regression was performed both without a fixed θ value, providing an un-normalized set of k_s and θ values for all watersheds, and using the average study area θ value of 0.38 to generate a normalized set of k_s values (e.g., Snyder et al., 2000, Kirby et al., 2003).

Watershed Profile Selection

Previous studies generally concur that the minimum drainage area required to form a bedrock channel ranges from approximately 10^5 m^2 to 1 km^2 (Montgomery and Foufoula-Georgiou, 1993; Sklar and Dietrich, 1998; Snyder et al., 2000; Montgomery, 2001). For our analysis of bedrock channel profiles, the start of a bedrock channel was selected individually based on the log of bin-averaged area-slope data within this accepted range of watershed areas. Channel profile slopes less than 2% were considered

to be artifacts of DEM preparation (such as may result from sink filling and channel calculation) and were excluded from further analysis. Similarly, channel profiles that deviated significantly from the expected log-linear fluvial profiles (Howard et al., 1994; Stock and Montgomery, 1999, Snyder et al., 2000; Montgomery, 2001, Snyder et al., 2003) were screened from further analysis (Figure 4 shows examples of selected and rejected channels). Of the 65 watersheds initially selected in the study area, 42 were ultimately selected based on the criteria established for further analysis.

Table 1. Isochron values which were used to calculate exhumation rates based on mineral cooling ages of Apatite fission track, (U-Th)/He Zircon, and $^{40}Ar/^{39}Ar$ Biotite methods. Calculated exhumation rates in mm yr^{-1} are shown to right of each age column.

Apatite Age (Ma)	Calculated Exhumation (mm yr^{-1})	Zircon Age (Ma)	Calculated Exhumation (mm yr^{-1})	Biotite (Ma)	Calculated Exhumation (mm yr^{-1})
<1	**>3**	<1	**>3**	<5	**>3**
1-5	**1-3**	1-5	**1-3**	5-10	**1-3**
5-10	**0.5-1**	5-10	**0.5-1**	10-20	**0.5-1**
10+	**<0.5**	10+	**<0.5**	20+	**<0.5**

Table 2. Exhumation rates in mm/yr based on all three mineral cooling ages. Placement of exhumation rate contours in Figure 4 are approximate, but sufficient to discriminate exhumation regimes in region for the purposes of this study.

Combined Exhumation Rate (mm yr^{-1})	Exhumation Classification
>3	**Rapid**
1-3	**Moderate**
.5-1	**Slow**
.1-.5	**Very Slow**

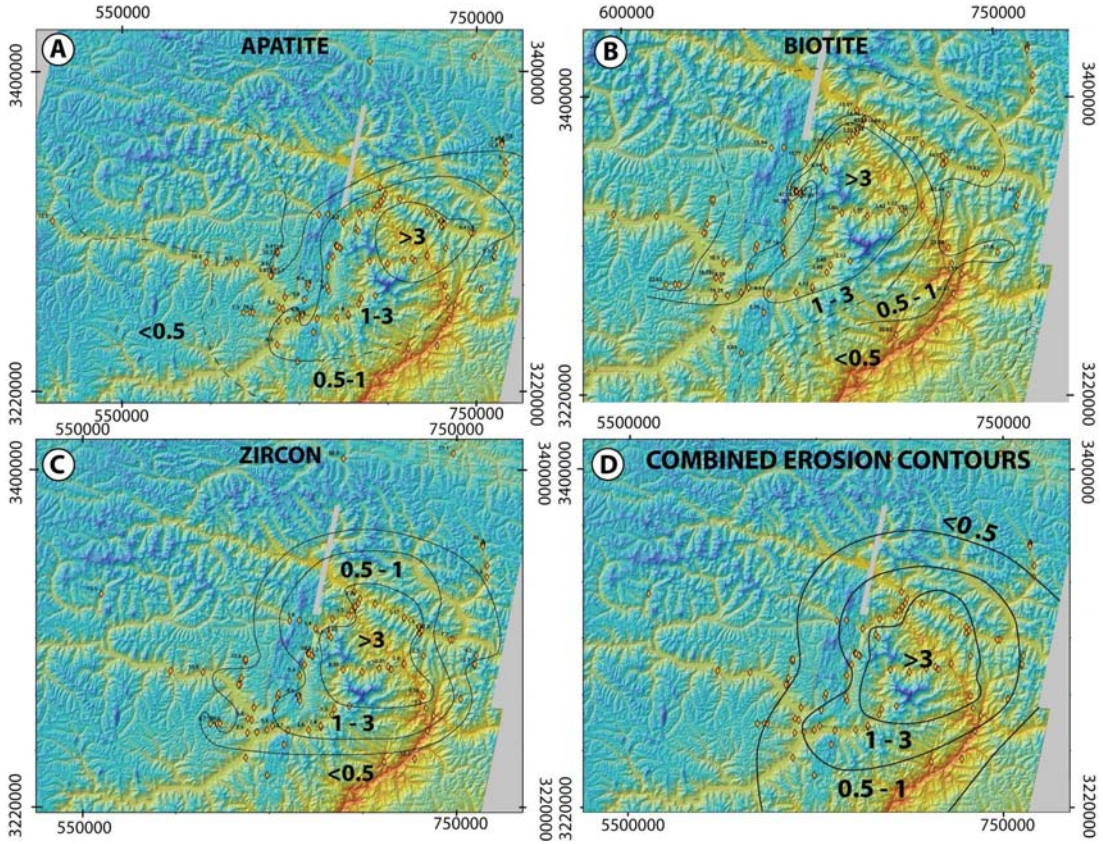

Figure 2. Exhumation rates shown in mm yr^{-1} calculated from mineral cooling age isochrons. A. Exhumation rates calculated based on Apatite cooling ages. From center, contour ages are <1 Ma, 1-5 Ma, 5-10 Ma and 10+ Ma. B. Exhumation rates based on Biotite cooling ages. From center, contour ages are <1 Ma, 1-5 Ma, 5-10 Ma and 10+ Ma. C. Exhumation rates based on Zircon cooling ages. From center, contour ages are <5 Ma, 5-10 Ma, 10-20 Ma and 20+ Ma. D. Contours showing exhumation rate spatial distribution are based on all three methods of dating. Contour locations are approximate, but provide sufficient means to distinguish the exhumation regimes between watersheds and assess the influence of tectonics on θ and k_s values (see text for details). Light regions indicate no DEM data was available. Mineral cooling data provided by P. Zeitler.

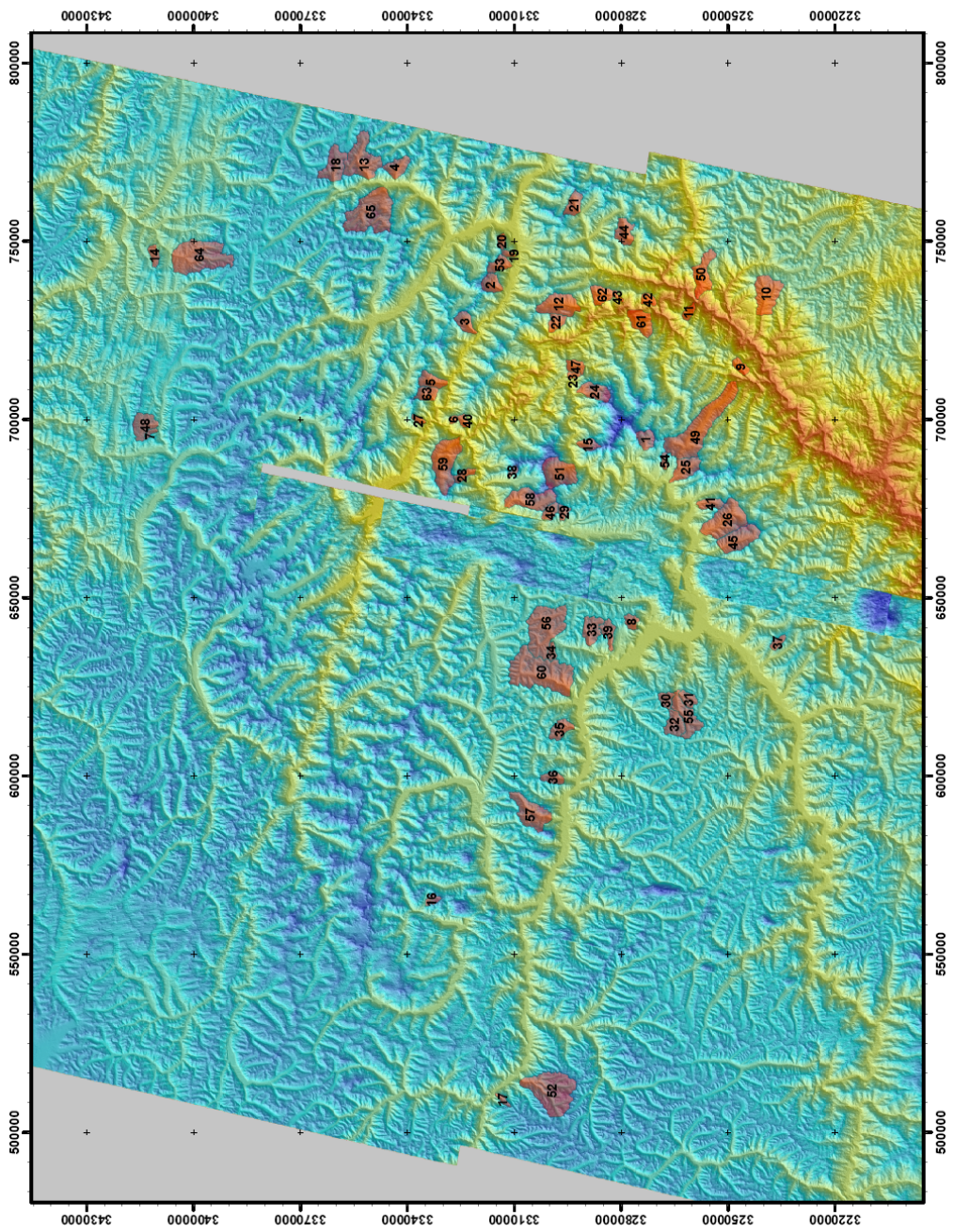

Figure 3. Map of selected watersheds used for analysis in Namche Barwa. Grey areas did not have DEM data available.

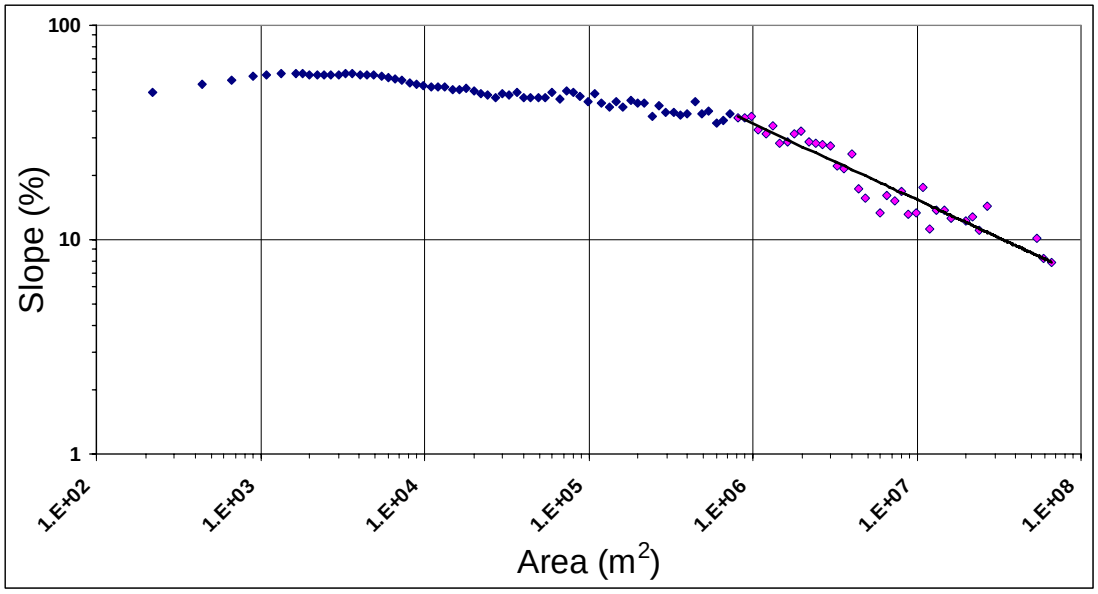

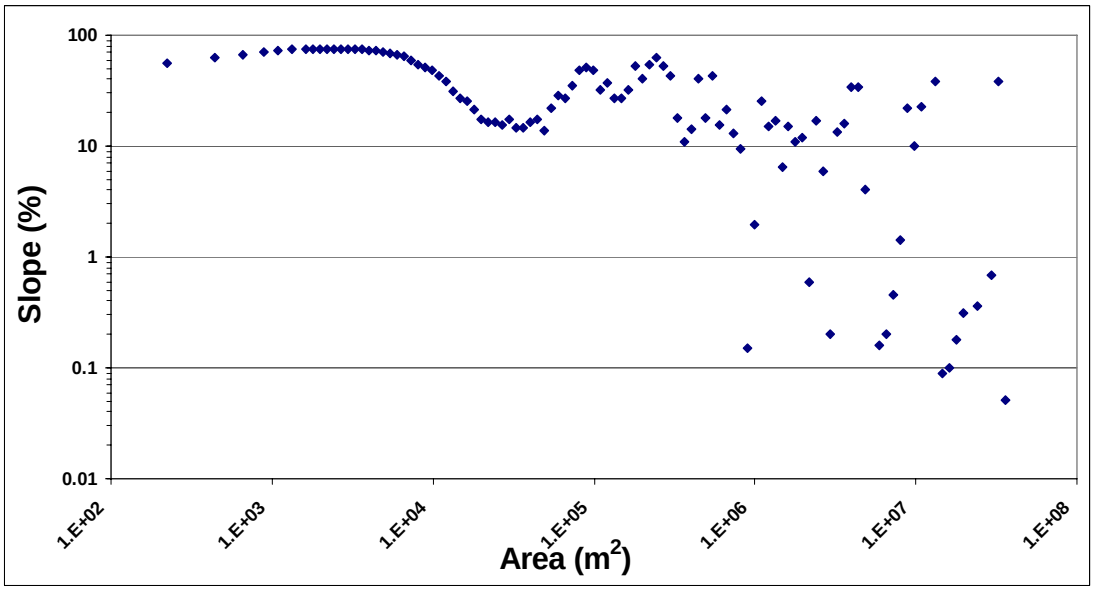

Figure 4. Two watershed area-slope plots. Top panel shows a bedrock channel profile which met the criteria for analysis (see text). Dark blue points are log binned data from original watershed data cloud, pink points constitute the bedrock channel within the watershed. Bottom panel shows profile that was screened from analysis based on a clearly non-fluvial profile.

Bedrock Incision Modeling

Background: Incision Modeling Parameters

Incision rates of bedrock channels are generally considered to determine the rate at which a landscape can be lowered in response to tectonic uplift, changes in climatic conditions or other basal adjustments as the final mechanism that removes eroded rock and cover from a region (e.g., Stock and Montgomery, 1999; Whipple and Tucker, 1999; Snyder et al., 2000; Whipple et al., 2000a; 2000b; Sklar and Deitrich, 2001; Snyder et al., 2003). Previous studies of bedrock erosion have focused on the parameterization of environmental variables to formulate an appropriate model that scales with tectonic activity, relief, watershed size and changes in lithology (e.g., Howard et al., 1994; Stock and Montgomery, 1999; Snyder et al., 2000, Lave and Avouac, 2001; Montgomery and Brandon, 2002; Snyder et al., 2003; Finnegan et al., 2005; Binnie et al. 2007).

Bedrock channel incision is commonly modeled using drainage area as a proxy for discharge, and channel slope, and a dimensional coefficient giving the familiar equation

$$\varepsilon = KA^{m}S^{n} \tag{2}$$

were ε is erosion rate, S is channel slope, A is watershed area and the K is the dimensional coefficient of erosion. Stock and Montgomery (1999) suggested that K is primarily set by bedrock lithology but variously it has been used to account for the influence of climate, sediment load, and tectonic environment (e.g., Sklar and Dietrich, 1998; Stock and Montgomery, 1999; Whipple and Tucker, 1999; Snyder et al., 2000; Whipple et al., 2000b). The exponents m and n are positive values that parameterize the influence of erosional processes, changes in channel width with drainage area and other

regional discharge-drainage area scaling relationships (Stock and Montgomery, 1999; Snyder et al., 2000; Whipple et al., 2000a).

For an erosional steady-state condition, and assuming the shear stress necessary to initiate erosion is negligible, the equation for bedrock incision can be recast for channel slope as a function of drainage area

$$S = k_s A^{-\theta} \quad (3)$$

where S is channel slope, k_s is regional uplift rate over the coefficient of erosion (given by $(U/K)^{1/n}$) and θ is equal to m/n. Under these assumptions, the θ value is thus representative of the dominant erosional process and hydrologic conditions, as expressed in the concavity of the channel.

The relationship seen in equation (3) leads to covariance between the variables k_s and θ for regressions performed on individual area-slope plots (Sklar and Dietrich, 1998; Snyder et al., 2000). Hence, small changes of the θ value in a regression can result in large differences in k_s values that makes meaningful comparison difficult between watersheds (e.g., Sklar and Dietrich, 1998; Snyder, 2000; Kirby et al, 2003). To control for this covariation, previous studies have calculated a normalized k_s value using either a fixed θ (typically done by adopting the average of unconstrained θ values from the individual channel networks) or by normalizing by a representative area for all watersheds during regression (Sklar and Dietrich, 1998; Snyder et al., 2000). This normalization is intended to allow interbasin comparison of steepness by removing the dependence of k_s on θ. Assuming the channel has reached erosional steady-state, and that the exhumation and K value for each channel is constant throughout the reach analyzed, k_s values can then be used to examine spatial patterns in exhumation for a study area.

In a previous study of the influence of m and n values on K, Stock and Montgomery (1999) compared paleochannel profiles with modern steady state profiles, which allowed calculation of an erosion rate. These erosion rates were then used in a numerical analysis that optimized the calculated channel profile to match the modern steady-state profile, yielding optimized m, n and K values for each channel. Their results indicated that in bedrock channels m/n values ranged from 0.3 to 0.5. In contrast, the value of K varied by more than five orders of magnitude depending on channel lithology, which ranged from highly erodible siltstones to harder, more resistant igneous rocks (e.g., Hawaiian basalt). In a similar study on the Upper Ukak River, Alaska, Whipple et al. (2000b) concluded that the value of K was dominated by the lithology of the bedrock within which the channel is located in. However, K may also be influenced by other erosional processes in addition to traditional bedrock incision such as mechanical frost wedging and sand blasting during low flow periods.

Snyder et al. (2000) found that using the model of bedrock incision and slope as described by equations (2) and (3), and presuming both uniform K value within a drainage and constant erosion process through time for the drainage channel, changes in tectonic regimes were correlated with changes in K as well as k_s. However no correlation was found between changes in uplift and θ value. In the same setting Snyder et al. (2003) later concluded that by varying the threshold shear stress for erosion, a constant K might apply throughout the same region (Snyder et al., 2003).

Applications of equations (2) and (3) to bedrock channels typically report θ values from 0.3 to 0.6 irrespective of tectonic environment (e.g., Whipple and Tucker, 1999; Snyder et al., 2000; Whipple et al., 2000a; Kirby et al., 2003; Montgomery and Lopez-

Blanco, 2003), although lower θ values ranging from 0.1 to 0.3 have been reported for debris-flow-dominated colluvial channels (Montgomery, 2001). This relatively narrow range of reported θ values, together with the strong covariance of θ and k_s, has resulted in θ being repeatedly normalized under the assumption that erosive processes do not change in a given channel reach. Here we show that the change in observed θ values is both predictable and significant in determining an appropriate k_s value for bedrock channels, and that the range of θ values spans from values for debris flow to fluvial dominance of bedrock incision.

Data Analysis and Interpretation

Our bedrock profile analysis yielded a log-linear relationship between θ and k_s values of the form

$$k_s = 2 \times 10^6 \times \theta^{5.6} \text{ (units } m^{2m}) \quad (4)$$

in which the correlation coefficient of $R^2 = 0.94$ indicates this model to be a strong first-order characterization of river profiles in the Namche Barwa region (Figure 5). Exhumation rates are distributed along the curve in a manner that does not show any significant stratification between populations. Similarly, spatial mapping of θ and k_s values in the study area demonstrated low θ and low k_s values were found in both areas of rapid exhumation and slow exhumation, while moderate to high θ and k_s values were found in all but the slowest exhumation regime (Figure 7). Normalization of k_s values following the methods of Sklar and Dietrich (1998) and Snyder et al. (2000) using a fixed θ value based on the study area average of 0.38 does not reveal any additional relationships between k_s, θ and calculated exhumation rates (Figure 6).

The strong correlation between k_s and θ values observed in this analysis validates the theoretical solution set of possible bedrock channel values predicted by Sklar and Deitrich (1998) that define a positive correlation between k_s and θ values. More specifically, Sklar and Dietrich (1998) found mathematically that for a given value of θ, k_s had a range of roughly one order of magnitude; creating an envelope of values in which bedrock channels were found. This covariance is expressed in the positive correlation between the two variables throughout all river systems where the model applies. Channels that were dominated by either all alluvial or debris flow processes were expected to plot beyond the bracketed range of θ and k_s values. Our data confirm the form of this predicted relationship over a range of watershed sizes and exhumation rates.

The strong correlation of θ and k_s values through both the fluvial and colluvial θ ranges (from $\approx$0.1 to >0.06) suggests a gradational continuum between the dominance of debris flows and fluvial bedrock channel processes on incision. Such an exchange may undermine the the key assumption that the shear stress needed for erosion is negligible, implicitly conceptualizing continuous, steady erosion through time. This assumption is incorporated indirectly in many models during the normalization process when θ is fixed to calculate k_s, implying a single continuous erosive process.

In reality, however, erosion is seldom a smooth, continuous process in mountain channel networks. While some channel erosion may occur due to dissolution, abrasion and cavitation (Whipple et al., 2000a), bedrock channel profiles also reflect intermittent large discharge and/or debris flow events with considerably more erosive power and transport capacity than average flows. We hypothesize that the range of k_s and θ values

we observe result from time averaging of these intermittent highly erosive events with less effective but more continuous erosive processes. We therefore consider it inappropriate to assume a single continuous erosion process dominates the channel, as has been previously assumed (e.g., Snyder et al., 2000; Kirby et al, 2003). Moreover, the distribution of high and low exhumation rates throughout the observed range of θ and k_s does not support a direct link between channel steepness (k_s) and tectonic regime.

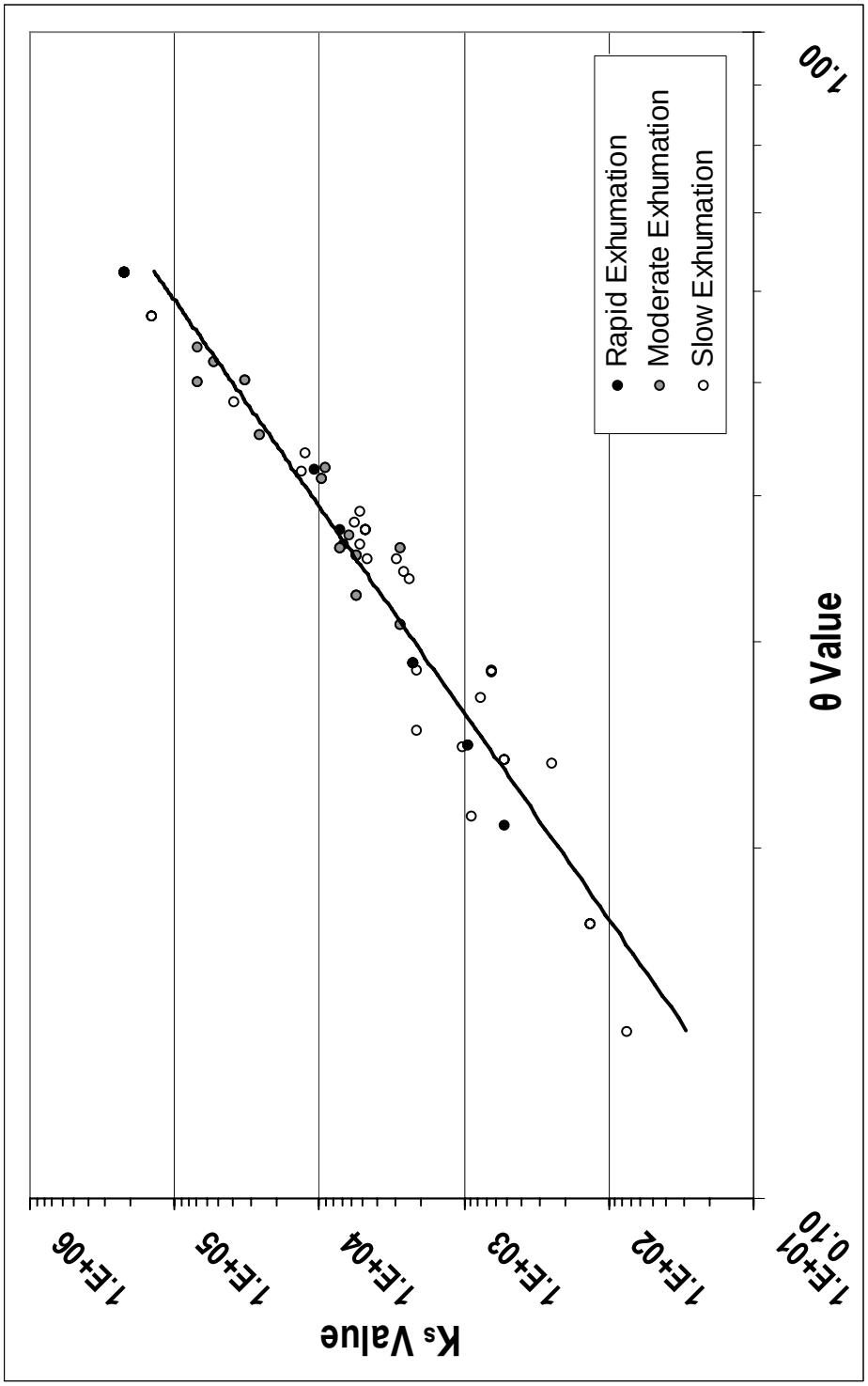

Figure 5. k_s values as a function of θ values. Regression line ($k_s = 2 \times 10^6 \theta^{5.7}$; R^2=0.94). Exhumation rates are based on mineral-cooling age data in study area (see text for details).

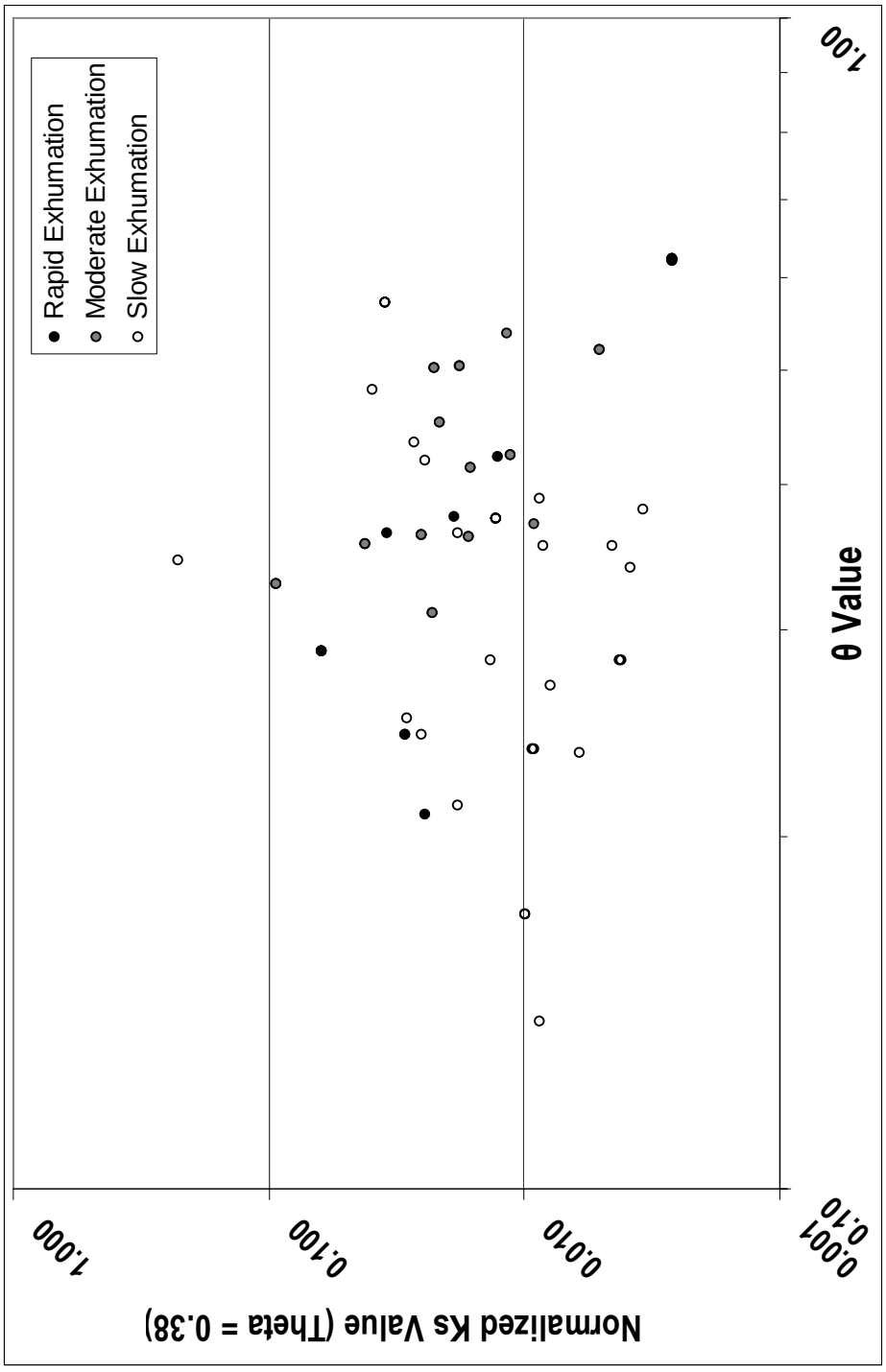

Figure 6. Normalized k_s values for $\theta = 0.38$.

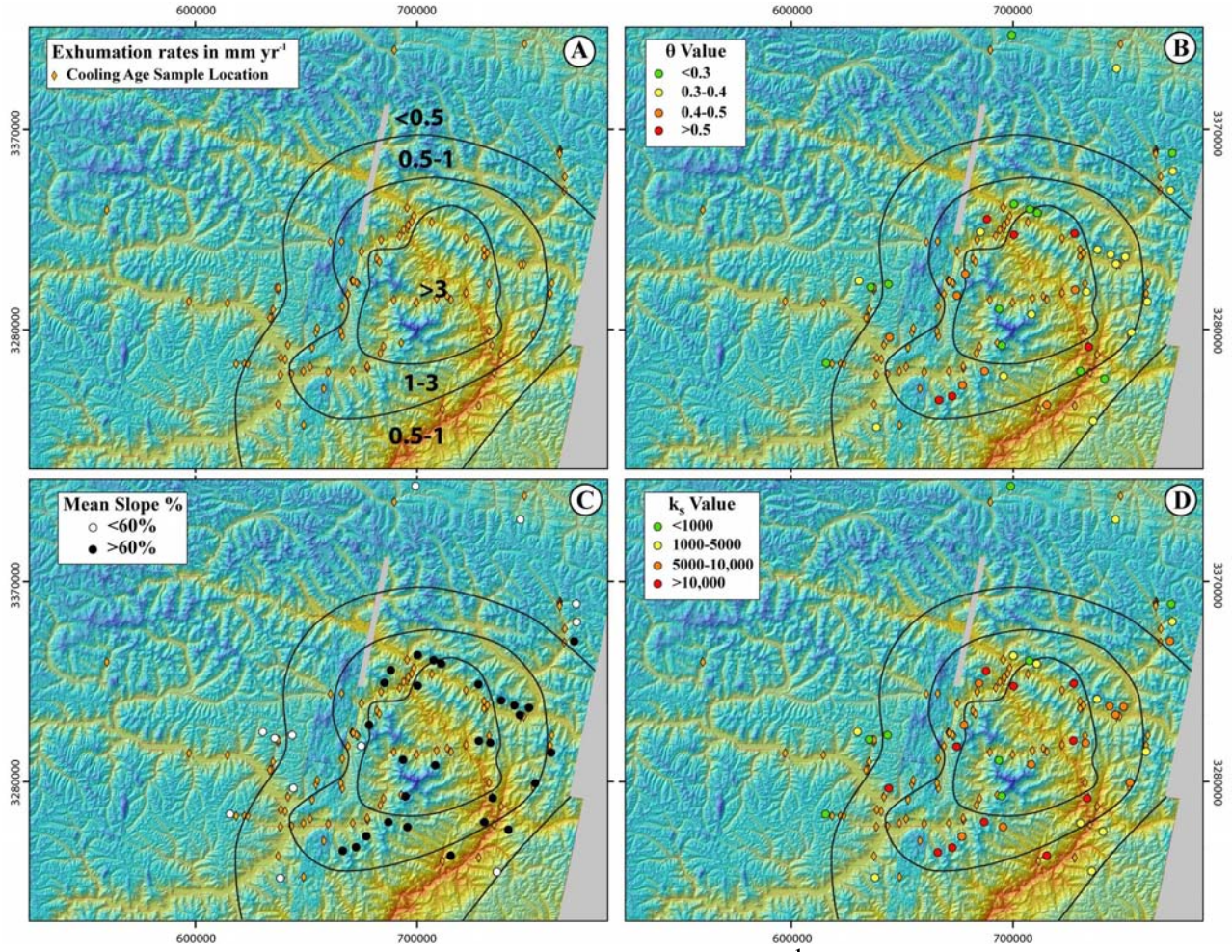

Figure 7. A) Exhumation rates calculated using mineral cooling ages in mm yr^{-1}. B) Spatial distribution of θ values in all exhumation regimes. C) Mean watershed slope spatial distribution over exhumation regimes, threshold hillslopes are found in higher exhumation rate areas. D) Spatial distribution of un-normalized k_s values in all exhumation regimes. High and low k_s and theta values are observed in the most rapid exhumation zone as well as in the zone of .5 – 1 mm yr^{-1}

Threshold Slope Development

Background: Development of Threshold Slopes

Considerations of the interplay between bedrock incision and landscape development has helped to produce the concept of threshold slopes, wherein hillslopes reach both a maximum gradient and relief regardless of rock uplift rate. Landscape development begins with regional uplift that initiates denudation. Where rocks weather and erode at rates comparable to the rate of rock uplift, a balance is reached between the rate of hillslope surface weathering and the rate of material removal by fluvial channels (Burbank et al., 1996; Montgomery, 2001; Binnie et al., 2007). Such landscapes are generally termed transport-limited due to an abundance of weathered material available for transport off the hillslopes and into the channel where it is removed. In transport-limited landscapes, local lithology sets the rate of rock weathering and thus is reflected in the hillslope gradients, which are coupled with changes in uplift and fluvial incision. As would be expected, friable lithologies result in lower gradient hillslopes whereas more erosion-resistant lithologies result in steeper gradients (Montgomery, 2001).

Threshold, or detachment-limited slopes result from rapid uplift increasing hillslope relief to a point where further bedrock incision by a basal channel leads to slope instability (Burbank et al., 1996). Intermittent landsliding limits the relief of the landscape and the frequency of sliding is determined by the rate of uplift and rate of bedrock incision (Montgomery and Brandon, 2002). Rapid exhumation leads to more frequent landsliding, whereas slower uplift reduces slide frequency. While some lithologic signature may be detected in threshold hillslope gradient, these slopes no longer track with changes in uplift or fluvial incision. Rather, as relief develops, hillslope

gradients increase to a maximum of typically between roughly 30° and 40° and are held at that angle by intermittent landsliding as fluvial incision continues (Burbank et al., 1996, Montgomery, 2001; Binnie et al., 2007).

Data Analysis and Interpretation

Our analysis found a relatively strong correlation ($R^2 = 0.75$) between mean hillslope gradient and k_s values up to a threshold gradient of approximately 60%, which corresponds to a 30° slope (Figure 7). The relationship between k_s and mean hillslope gradient below 30° can be described using a power function of the form

$$k_s = 2 \times 10^{-10} S^{7.68} \text{ (units } m^{2m}) \quad (5)$$

Not surprisingly gentle hillslope gradients (i.e., those <60%) were located in slow exhumation regions of the study area and steeper slopes were concentrated in the moderate to rapid exhumation regions (Figure 7). At slopes greater than 60%, no relationship is discerned between k_s and mean hillslope gradient.

The log-linear relationship between mean hillslope gradient values less than 30° and channel steepness k_s affirms previous findings: that for highly erodable (low K value) channels in slow exhumation environments, surrounding hillslope gradients reflect the influence of rock uplift rate and lithology, and are coupled with changes in the rate of channel incision (Burbank et al., 1996; Montgomery, 2001; Montgomery and Brandon, 2002; Binnie et al., 2007; Korup et al., 2007). In contrast, the lack of relationship between k_s and hillslope gradient beyond 30° supports the idea that at high exhumation rates, threshold hillslope gradients develop which are no longer coupled with changes in

fluvial incision but remain at a threshold value and intermittent mass wasting to limits further relief development.

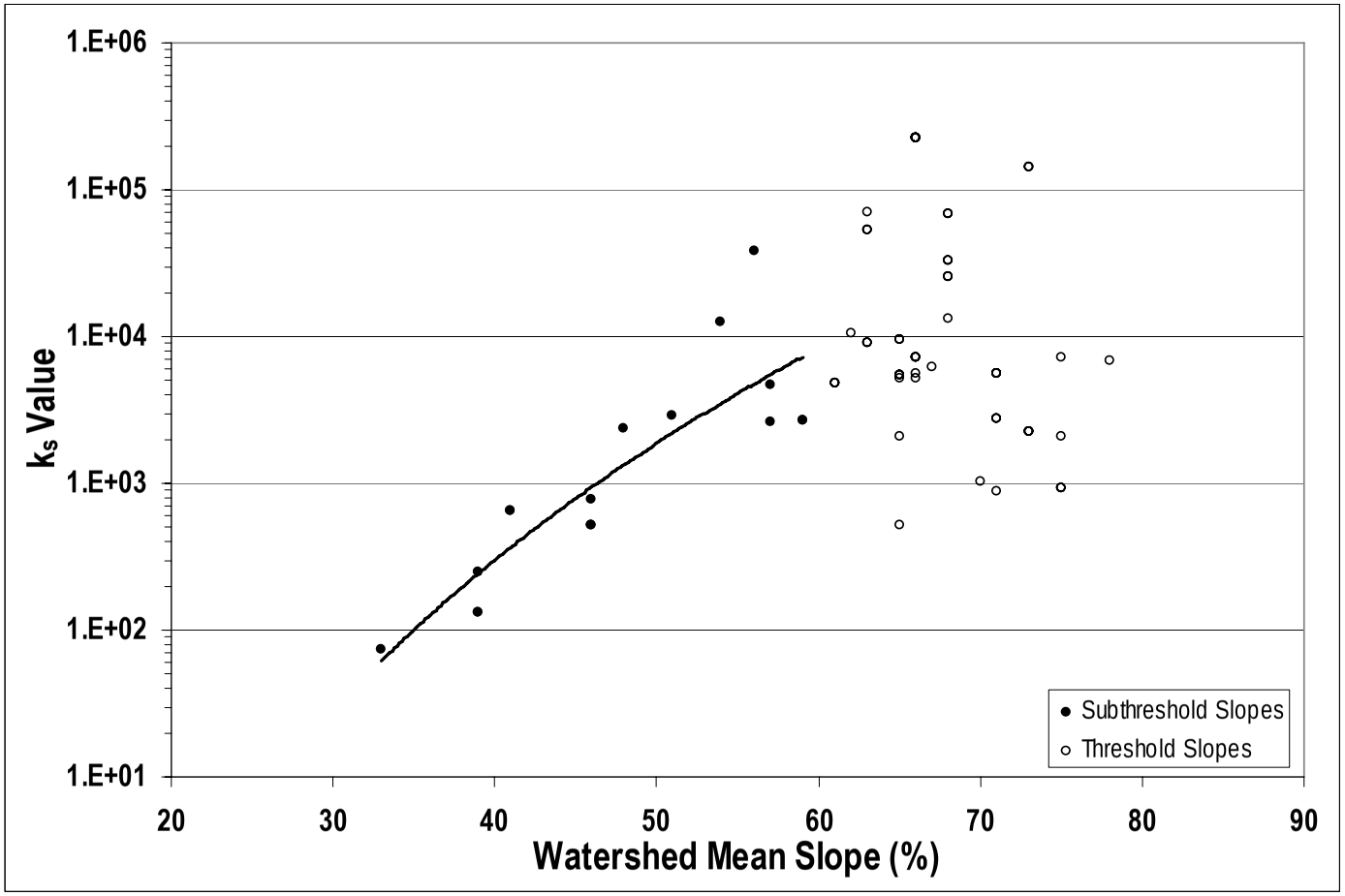

Figure 8. Mean hillslope gradient versus k_s value for all watersheds. Regression line ($k_s=2 \times 10^{-11}S^{8.2}$) is based on black data points and includes hillslope gradients up to 61% ($R^2=0.75$); hollow points constitute threshold slope values and are not part of regression. The maximum correlation between k_s and hillslope gradient ($R^2=0.85$) is reached at a gradient of 56%. We hypothesize that the break in processes between threshold and subthreshold systems begins at a slope of about 30 degrees (60%) based on the distribution of current data and so use this number for discussion. Note that for any suite of channels, the time of analysis may yield a slightly different break between populations due to the unpredictable nature of when landslides, which adjust relief and hillslope gradient, occur.

Conclusions

Stream profile analysis using un-normalized data from a wide range of watersheds suggests erosive processes in bedrock channels are well represented as a gradational transition between debris flow and fluvial erosion. This transition is observed as a smooth log-linear function between θ and k_s values, which range across the spectrum of values expected to characterize bedrock and debris-flow channels. Moreover, new mineral-cooling data combined with stream profile analysis suggests that k_s values are not directly correlated with rock uplift rates because watersheds with high exhumation rates are spread evenly along the curve of k_s versus θ. In addition the strong correlation between mean hillslope gradient and channel k_s values up to about 30°, reflects expectations for subthreshold, transport-limited landscapes wherein hillslope gradients and channel morphology are closely coupled. In steeper terrain, mean hillslope gradients show no correlation with channel steepness k_s and instead support the idea that hillslope gradients become decoupled from the rate of fluvial incision, remaining at a maximum gradient of between 30° and 40° which is maintained through intermittent landsliding.

References

Binnie, S. A., W. M. Phillips, M. A. Summerfield and L. K. Fifield (2007). "Tectonic uplift, threshold hillslopes and denudation rates in a developing mountain range." Geology 35 (8): 743 - 746.

Burbank, D. W., J. Leland, E. Fielding, R. S. Anderson, N. Brozovic, M. R. Reid and C. Duncan (1996). "Bedrock incision, rock uplift and threshold hillslopes in the northwestern Himalayas." Nature 379: 505-510.

Finlayson, D. P., D. R. Montgomery and B. Hallet (2002). "Spatial coincidence of rapid inferred erosion with young metamorphic mssifs in the Himalayas." Geology 30 (3): 219 - 222.

Finnegan, N., G. Roe, D. R. Montgomery and B. Hallet (2005). "Controls on the channel width of rivers: Implications for modeling fluvial incision of bedrock." Geology 33 (3): 229 - 232.

Galy, A. and C. France-Lanord (2001). "Higher erosion rates in the Himalaya: Geochemical constraints on riverine fluxes." Geology 29 (1): 23 - 26.

Grove, M. and M. T. Harrison (1996). "40Ar diffusion in Fe-rich biotite." American Mineralogist 81: 949-951.

Harrison T.M., O.M. Lovera, M. Grove (1992). "New insights into the origin of two contrasting Himalayan granite belts." Geology 25 (10), p. 899-902.

Howard, A. D., W. E. Deitrich and M. A. Seidl (1994). "Modeling fluvial erosion on regional to continental scales." Journal of Geophysical Research 99 (No. B7): 13,971 - 13,986.

Kirby, E., K. X. Whipple, W. Tang and Z. Chen (2003). "Distribution of active rock uplift along the eastern margin of the Tibetan Plateau: Inferences from bedrock channel longitudinal profiles." Journal of Geophysical Research 108 (No. B4), pp. 10.

Korup, O., J. J. Clague, R. L. Hermanns, K. Hewitt, A. L. Strom and J. T. Weidinger (2007). "Giant landslides, topography, and erosion." Earth and Planetary Science Letters 261: 578-589.

Lave, J. and J. P. Avouac (2001). "Fluvial incision and tectonic uplift across the Himalayas of central Nepal." Journal of Geophysical Research 106 (No. B11): 26,561 - 26,591.

Montgomery D.R. and E. Foufoula-Georgiou (1993). "Channel network sources representation using digital elevation models." Water Resources Research, 29: 3925-3934.

Montgomery, D. R. (2001). "Slope distributions, threshold hillslopes and steady-state topography." American Journal of Science 301: 432-454.

Montgomery, D. R. and M. T. Brandon (2002). "Topographic controls on erosion rates in tectonically active mountain ranges." Earth and Planetary Science Letters 201: 481 - 489.

Montgomery, D. R. and J. Lopez-Blanco (2003). "Post-Oligocene river incision, southern Sierra Madre Occidental, Mexico." Geomorphology 55: 235 - 247.

Reiners, P. W., K. A. Farley and H. J. Hickes (2002). "He diffusion and (U-Th)/He thermochronometry of zircon; initial results from Fish Canyon Tuff and Gold Butte." Tectonophyics 349: 297-308.

Sklar, L. S. and W. E. Dietrich (1998). “River longitudinal profiles and bedrock incision models: Stream power and the influence of sediment supply.” AGU Geophysical Monograph 107, 237-260. Tinkler and Wohl, AGU Washington D.C..

Sklar, L. S. and W. E. Dietrich (2001). "Sediment and rock strength controls on river incision into bedrock." Geology 29 (12): 1087-1090.

Snyder, N. P., K. X. Whipple, G. E. Tucker and D. J. Merritts (2000). "Landscape response to tectonic forcing: Digital elevation model analysis of stream profiles in the Mendocino triple juncion region, northern California." GSA Bulletin 112 (No. 8): 1250 - 1263.

Snyder, N. P., K. X. Whipple, G. E. Tucker and D. J. Merritts (2003). "Channel responses to tectonic forcing: field analysis of stream morphology and hydrology in the Mendocino triple junction region, northern California." Geomorphology 53: 97 - 127.

Stock, J. D. and D. R. Montgomery (1999). "Geologic constraints on bedrock river incision using the stream power law." Journal of Geophysical Research 104 (B3): 4983 - 4993.

Stuwe, K. (2002). Geodynamics of the Lithosphere. Berlin; New York, Springer.

Tarboton, D. G., R. L. Bras and I. Rodriguez-Iturbe (1989). "Scaling and elevation in river networks." Water Resourches Research 25 (9): 2037 - 2051.

Tarboton, D. G., R. L. Bras and I. Rodriguez-Iturbe (1991). "On the extraction of channel networks from digital elevation data." Hydrological Processes 5: 81 - 100.

Warnock, A. C., P. K. Zeitler, R. A. Wolf and S. C. Bergman (1997). "An evaluation of low temperature apatite U-Th/He thermochronometry." Geochemica et Cosmochimica Acta, 61 (No. 24): 5371 - 5377.

Whipple, K. X., G. S. Hancock and R. S. Anderson (2000a). "River incision into bedrock: Mechanics and relative efficacy of plucking, abrasion, and cavitation." GSA Bulletin 112(3): 490 - 503.

Whipple, K. X., N. P. Snyder and K. Dollenmayer (2000b). "Rates and processes of bedrock incision by the Upper Ukak River since the 1912 Novarupta ash flow in the Valley of Ten Thousand Smokes, Alaska." Geology 28 (9): 835-838.

Whipple, K. X. and G. E. Tucker (1999). "Dynamics of the stream-power river incision model: Implications for height limites of mountain ranges, landscape response timescales and research needs." Journal of Geophysical Research 104 (No. B8): 17,661 - 17,674.

Zeitler, P. K., A. S. Meltzer, P. O. Koons, D. Craw, B. Hallet, C. P. Chamberlain, W. S. F. Kidd, S. K. Park, L. Seeber, M. Bishop and J. Shroder (2001). "Erosion, Himalayan geodynamics, and the geomorphology of metamorphism." GSA Today 11 (1): 4-9.

Appendix A: Full Watershed Data

	Sample	Elevation (m)	Longitude			Latitude			Apatitie U-Th/He			Zircon U-Th/He			Biotite $^{40}Ar/^{39}Ar$			BASIN GRID NUMBER	Theta	K_s	Basin Mean Slope	Basin Area (m^2)	Calculated Channel Slope
									n[1]	Age (Ma)[2]	± 2σ	n[1]	Age (Ma)	± 2σ	Age (Ma)[3]	± 2σ	MSWD[4,5]						
Distal samples																							
	CL-04-05	3635	95°	35.777'	30°	46.977'			2			2	77.1	59				64	0.340	2351	48	1.083E+08	4.34
	CL-06-05	4208	94°	58.913'	30°	46.168'						2	50.5	9.1				48	0.139	73	33	3.603E+07	6.50
Bomi Region																							
*	BC-03-02	2968	95°	54.943'	29°	47.018'	2	30.3	17.1	2	12.3	2.3	44.08	1.47	>100			40	0.572	144143	73	8.886E+06	15.23
*	BC-03-02	2968	95°	54.943'	29°	47.018'	2	30.3	17.1	2	12.3	2.3	44.08	1.47	>100			59	0.623	223225	66	8.040E+07	2.64
	BM-01-05	3054	95°	45.997'	30°	11.113'				2	10.9	1.8						4	0.364	5209	65	2.186E+07	11.08
	BM-02-02	3646	95°	41.857'	29°	48.556'				2	9.2	1.4	22.45	0.29	14.5			21	0.375	4789	61	2.415E+07	8.21
	BM-02-05	3762	95°	44.942'	30°	20.340'	2	8.7	0.6									18	0.238	519	46	4.864E+07	7.64
	BM-03-02	4286	95°	41.111'	29°	45.886'				2	10.3	1.5						21	0.375	4789	61	2.415E+07	8.21
	BM-04-05	4059	95°	44.920'	30°	20.837'	2	7.8	0.5									18	0.270	771	46	4.864E+07	6.51
	BM-05-02	4321	95°	41.297'	29°	46.135'	4	6.3	5.5									21	0.375	4789	61	2.415E+07	8.21
	BM-06-05	4359	95°	45.040'	30°	21.042'	2	12.8	5.7	2	36	4.2						18	0.238	519	46	4.864E+07	7.69
	NBK-41-23	3207	95°	46.199'	30°	14.447'	2	8	0.6									13	0.345	2611	57	4.036E+05	30.39
SE of NB-GP Massif																							
	b-115	1900	95°	24.825'	29°	33.825'				2	1.2	0.4						42	0.505	32763	68	1.199E+07	8.73
	b-143	4100	95°	36.376'	29°	36.100'							17.8	0.29	0.5			44	0.390	5225	66	3.261E+07	6.19
	b-35	1059	95°	20.713'	29°	19.197'				2	12.1	2.7						10	0.355	4653	57	6.566E+07	7.88
	b-376	1021	95°	27.252'	29°	31.514'							15.57	0.24	2.6			42	0.505	32763	68	1.199E+07	8.73
*	b-45	905	95°	25.161'	29°	27.230'							35.85	1.01	5.3			50	0.253	2097	65	4.864E+07	23.94
*	b-45	905	95°	25.161'	29°	27.230'							35.85	1.01	5.3			11	0.284	2097	75	6.566E+07	12.61
*	b-77	990	95°	10.590'	29°	18.540'							20.82	0.69	4.5			9	0.420	13205	68	1.465E+07	12.83
*	b-77	990	95°	10.590'	29°	18.540'							20.82	0.69	4.5			49	0.381	5587	66	1.461E+08	4.33
Northern Margin, NB-GP Massif																							
*	b-188	3290	95°	24.300'	29°	48.850'				2	2.3	1.3	43.44	0.43	>100			22	0.453	25612	68	1.978E+07	12.68
*	b-188	3290	95°	24.300'	29°	48.850'				2	2.3	1.3	43.44	0.43	>100			12	0.371	6229	67	5.941E+07	8.19
*	BC-01-05	2695	95°	34.111'	29°	53.325'	4	1.4	0.5	1	7.7	0.9						20	0.356	5491	65	8.886E+06	18.36
*	BC-01-05	2695	95°	34.111'	29°	53.325'	4	1.4	0.5	1	7.7	0.9						19	0.329	5521	71	5.390E+06	33.52
*	BC-01-05	2695	95°	34.111'	29°	53.325'	4	1.4	0.5	1	7.7	0.9						53	0.362	7117	66	2.186E+07	15.58
	BT-01-03	2027	95°	01.935'	30°	03.431'									4.7	0.07	13.5	59	0.623	223225	66	8.040E+07	2.65
	BT-07-02	2485	94°	48.697'	29°	57.253'	2	2.2	0.1	2	1.4	0.3	11.77	0.2	0.9			58	0.424	8953	63	2.186E+07	6.92
*	BT-08-03	2062	95°	03.558'	30°	05.628'							15.12	0.15	>100			59	0.623	223225	66	8.040E+07	2.64
*	BT-08-03	2062	95°	03.558'	30°	05.628'							15.12	0.15	>100			27	0.288	2243	73	6.583E+06	24.27
	BT-09-03	2051	95°	01.715'	30°	02.659'							3.22	0.03	41			59	0.623	223225	66	8.040E+07	2.65
*	BT-18-01	2109	95°	03.575'	30°	05.619'				2	0.36	0.17						59	0.623	223225	66	8.040E+07	2.64
*	BT-18-01	2109	95°	03.575'	30°	05.619'				2	0.36	0.17						27	0.288	2243	73	6.583E+06	24.27
*	BT-22E-02	2736	95°	33.275'	29°	53.344'	4	0.4	0.2				15.83	0.25	1.3			20	0.356	5491	65	8.886E+06	18.36
*	BT-22E-02	2736	95°	33.275'	29°	53.344'	4	0.4	0.2				15.83	0.25	1.3			53	0.362	7117	66	2.186E+07	15.58
*	BT-22E-02	2736	95°	33.275'	29°	53.344'	4	0.4	0.2				15.83	0.25	1.3			19	0.329	5521	71	5.390E+06	33.52
*	BT-23-02	2600	95°	23.072'	29°	57.244'	4	0.5	0.1	2	1.6	0.6	13.73	0.25	0.1			2	0.311	2728	71	2.186E+07	14.14
*	BT-23-02	2600	95°	23.072'	29°	57.244'	4	0.5	0.1	2	1.6	0.6	13.73	0.25	0.1			3	0.503	68110	68	2.186E+07	13.80
*	BT-24-02	2720	95°	18.119'	30°	00.053'				2	0.67	0.14	12.87	1.05	58.7			2	0.311	2728	71	2.186E+07	14.14

*	**BT-24-02**	2720	95°	18.119'	30°	00.053'				2	0.67	0.14	12.87	1.05	58.7	**3**	0.503	68110	68	2.186E+07	13.80
*	**BT-32-02**	2200	95°	08.611'	30°	04.088'							14.86	0.18	58.7	**63**	0.213	889	71	8.040E+07	18.31
*	**BT-32-02**	2200	95°	08.611'	30°	04.088'							14.86	0.18	58.7	**5**	0.245	1029	70	2.415E+07	16.08
	BT-35-02	2094	95°	01.734'	30°	07.675'							10.61	0.27	2.8	**27**	0.288	2243	73	6.583E+06	24.27
Namche Barwa – Gyala Peri Massif																					
	b-232	2713	94°	57.594'	29°	45.260'				2	0.26	0.2	1.66	0.05	1.1	**15**	0.245	937	75	1.619E+07	16.00
	b-237	2767	95°	03.909'	29°	44.542'							1.77	0.06	0.5	**15**	0.245	937	75	1.619E+07	16.00
	b-247	2748	95°	09.506'	29°	45.487'				4	0.7	1	3.43	0.09	3.1	**24**	0.376	7139	75	2.415E+07	12.00
	b-265	1470	95°	17.850'	29°	46.700'				2	0.6	0.28				**22**	0.453	25612	68	1.978E+07	12.68
	BT-01-02	1995	95°	00.656'	30°	02.330'							1.68	0.17	0.9	**59**	0.623	223225	66	8.040E+07	2.64
	BT-05-02	2351	94°	54.298'	29°	59.999'							1.57	0.04	0.8	**28**	0.364	6826	78	1.326E+07	17.33
	GP-14-03	3600	94°	53.036'	29°	55.409'				2	0.83	0.3				**58**	0.424	8953	63	2.186E+07	6.92
	IG-11-01	4309	94°	59.436'	29°	34.827'							2.12	0.07	1.7	**1**	0.209	514	65	2.186E+07	15.01
	IG-15a-01	3113	94°	53.558'	29°	32.385'				2	1.3	0.2	2.45	0.06	0.4	**25**	0.422	10624	62	2.415E+07	8.09
Western Margin NB-GB Massif (Lulan Valley, De'u Gungbu section))																					
	BT-12-01	3267	94°	44.794"'	29°	46.914'							16.38	0.34	0.6	**29**	0.436	12502	54	8.886E+06	11.68
Tethyan and Mylonite Sequences, Northern Flank of Namche Barwa																					
	b-138	3760	94°	31.880'	29°	15.215'							5.89	0.1	0.6	**37**	0.362	2712	59	1.085E+07	7.69
	BT-01-01	2931	94°	38.958'	29°	28.024'				2	3.7	0.4	4.91	0.11	0.5	**45**	0.522	52591	63	5.941E+07	4.58
	GS149	3250	94°	37.661'	29°	23.930'							5.39	0.08	0.3	**45**	0.522	52591	63	5.941E+07	4.58
	IG-19-01	3057	94°	49.971'	29°	28.844'				2	2.4	0.6	4.12	0.1	0.2	**41**	0.415	9436	65	1.789E+07	9.29
*	**IG-20b-01**	3097	94°	45.763'	29°	28.099				2	2.9	0.3				**41**	0.415	9436	65	1.789E+07	9.29
*	**IG-20b-01**	3097	94°	45.763'	29°	28.099				2	2.9	0.3				**26**	0.538	69763	63	2.415E+07	7.40
	NBK-13-23	3070	94°	24.882'	29°	20.334'	3	4.5	2.2							**37**	0.362	2712	59	1.085E+07	7.69
*	**NBK-36-23**	2940	94°	49.846'	29°	29.291'	2	1.8	0.1							**20**	0.356	5491	65	8.886E+06	18.36
*	**NBK-36-23**	2940	94°	49.846'	29°	29.291'	2	1.8	0.1							**19**	0.329	5521	71	5.390E+06	33.52
*	**NBK-36-23**	2940	94°	49.846'	29°	29.291'	2	1.8	0.1							**53**	0.362	7117	66	2.186E+07	15.58
Nyang Watershed																					
*	**BL-09-03**	2954	94°	25.781'	29°	31.625'	2	9.1	3	2	9.3	1.1	18.75	0.22	8	**40**	0.572	144143	73	8.886E+06	15.23
*	**BL-09-03**	2954	94°	25.781'	29°	31.625'	2	9.1	3	2	9.3	1.1	18.75	0.22	8	**59**	0.623	223225	66	8.040E+07	2.64
	BT-04-01	3028	94°	27.821'	29°	34.734'							18.5	0.38	1.4	**8**	0.482	38551	56	8.886E+06	17.19
	BT-20E-02	3090	94°	11.051'	29°	45.132'	2	9.3	2.3	2	13.9	2.3				**60**	0.355	2894	51	8.040E+07	4.56
Higher Elevations Above Lower Nyang River																					
*	**BL-02-03**	3995	94°	25.349'	29°	48.663'	2	6.4	0.2							**34**	0.172	132	39	2.950E+07	6.79
*	**BL-02-03**	3995	94°	25.349'	29°	48.663'	2	6.4	0.2							**56**	0.284	647	41	6.566E+07	3.93
	BL-05-03	4258	94°	13.300'	29°	30.219'	2	7.3	0.4	2	8.7	1.2	22.63	0.23	70.1	**32**	0.237	247	39	2.950E+07	4.21
*	**NB02-120**	4080	94°	25.272'	29°	48.070'	1	10.3	0.5	2	13.6	2.2				**34**	0.172	132	39	2.950E+07	6.85
*	**NB02-120**	4080	94°	25.272'	29°	48.070'	1	10.3	0.5	2	13.6	2.2				**56**	0.284	647	41	6.566E+07	3.90

1 -- Number of replicates

2 -- Age calculated assuming no contribution from 147Sm

3 -- Uncertainty includes uncertainty in J-factor

4 -- For biotites with MSWD > 15, age and uncertainty reported are integrated over total gas release. If MSWD < 15, age and uncertainty are for inverse isochron.

5 -- 'm' following MSWD value indicates sample is a white mica, not

* INDICATES MULTIPLE WATERSHEDS FOR SINGLE AGE